Formation of Ordered Multilayers from Polyoxometalates and Silver on Electrode Surfaces

ARTICLE *in* THE JOURNAL OF PHYSICAL CHEMISTRY B · MAY 2004

Impact Factor: 3.3 · DOI: 10.1021/jp0494436

Formation of Ordered Multilayers from Polyoxometalates and Silver on Electrode Surfaces

Jongwon Kim,[†] Lien Lee,[†] Brian K. Niece,[†] Jia X. Wang,[‡] and Andrew A. Gewirth*,[†]

Department of Chemistry, and Frederick Seitz Materials Research Laboratory, University of Illinois at Urbana−Champaign, Urbana, Illinois 61801, and Materials Science Department, Brookhaven National Laboratory, Upton, New York 11973

Received: February 6, 2004; In Final Form: March 25, 2004

We show that multilayers of a common polyoxometalate—silicotungstic anion (STA), α-$SiW_{12}O_{40}^{4-}$—are formed on a Ag electrode surface or other electrode surfaces in the presence of Ag^+ poised in the cathodic potential region. This effect is not observed on either Au surfaces or C surfaces absent Ag^+. Surface X-ray scattering, quartz crystal microbalance, X-ray photoelectron spectroscopy, and scanning tunneling microscopy measurements show that the silicotungstic acid apparently stabilizes the Ag^+ cation, which electrostatically assembles with the STA anion or the one-electron reduced species to form ordered multilayers. In contrast to other electrostatically assembled multilayer systems, those formed here exhibit considerable order.

I. Introduction

The modification of electrode surfaces with polyoxometaltes (POMs) has been extensively studied for decades since POMs have many practical applications in areas such as heterogeneous catalysis,[1] electrocatalysis,[2] and corrosion inhibition.[3] One particular focus of work has been to immobilize the POM onto a surface, to incorporate the functionality available with a POM into a heterogeneous catalytic environment. In particular, considerable effort has also attended the formation of multilayers of POMs, since multilayers have many desirable features which aid in construction of functional materials such as electrochemical and electrocatalytic devices.[4−6]

There are several methods available to build multilayer structures consisting of POMs and cationic species. The most well investigated way is the so-called alternate immersion[7] or immersion growth method,[8] in which the electrostatic interaction between cations and anions plays a role as the driving force. In this method, approximately a monolayer of polyanions is first adsorbed on the electrode surface by immersing the electrode in the modification solution. After being modified with polyanions, the electrode is then exposed to the solution containing a large cation. By alternating immersion into the anionic and cationic solutions, the number of immobilized layers can be controlled. For example, glassy carbon,[7,9,10] Ag,[5] indium tin oxide, and Au[4] electrodes have been successfully modified with POMs to form multilayer structures.

Electrode surfaces modified with monolayers formed from aminoethanethiol on Au[11] or aminobenzoic acid on glassy carbon[12] can also be further modified to layer-by-layer assembly of multilayer films consisting of POM anions and a cationic polymer. In this case, aminoethanethiol and aminobenzoic acid monolayers provide a positively and negatively charged surface, respectively, which in turn interacts with the anionic and cationic species.

An alternative method developed to grow multilayers involves the use of potential cycling to affect the adsorption of POMs on electrode surfaces.[13−15] For example, the amount of immobilized polymolybdate on a carbon fiber microelectrode was found to increase continuously as potential scanning proceeded.[13] In some cases, pretreatment of carbon electrodes was necessary to activate the electrode to produce a uniform monolayer of POMs.[14,15] Cheng and co-workers utilized potential cycling in order to build multilayer films of silicomolybdates on a Au electrode precoated with cysteamine self-assembled monolayer.[8,16] Compared to the immersion method, multilayer self-assemblies formed using electrochemical treatments were found to be more uniform and stable.[17] Combinations of the electrochemical and immersion methods have also been examined.[18]

Efforts directed at forming multilayers of POMs on surfaces mirror the much larger effort dedicated to the formation of organic multilayers. As with inorganic multilayers, electrostatic interaction can be exploited to form organic multilayers (see ref 19 and references therein). However, a high surface charge density is necessary to induce the attraction between neighboring layers, primarily limiting this method to polyelectrolytes.[20] Other methods involve coordination between organic ligands and multivalent metal ions,[20−24] or the direct formation of covalent bonds between adjacent layers through the use of alkanedithiols [25−27] or C−N and Si−O linkages.[28]

In previous work, we showed that one of the polyoxometalates, α-dodecatungstosilicate anion (STA), α-$SiW_{12}O_{40}^{4-}$, spontaneously forms ordered monolayer arrays on Ag(111) surfaces from acidic aqueous solution.[29] In-situ STM images of the adsorbed monolayer on Ag(111) revealed that STA forms a 4-fold symmetric square adlattice on Ag(111), which was ascribed to an arrangement where the T_d-symmetric STA molecule was oriented with its S_4 axis perpendicular to the Ag(111) surface.[30,31] X-ray reflectivity measurements on the Ag(100) surface confirmed the S_4 axis orientation of the molecule with respect to the surface.[32] Interestingly, the Ag-surface-confined POM exhibits a unique electrochemical response relative to POMs immobilized on electrode surfaces by methods such as dipping and entrapment in a polymer matrix (see ref 33 and references therein). STA molecules on Ag surfaces passivate the electrode toward subsequent solution redox

* To whom correspondence should be addressed. Telephone: 217-333-8329. Fax: 217-333-2685. Email: agewirth@uiuc.edu.
[†] University of Illinois.
[‡] Brookhaven National Laboratory.

10.1021/jp0494436 CCC: $27.50
Published on Web 05/15/2004

chemistry, while surfaces modified with POMs using other methods yield voltammetric waves similar to those of the solution counterparts. Vibrational spectroscopic measurements indicate a strong interaction between POMs and the Ag electrode via both the bridging and terminal O groups of the molecules.[34,35] Although STA forms a monolayer on Au surfaces, the electrochemical response of Au is not affected by the adsorption of STA.[32]

The unique behavior on Ag surfaces provides an opportunity to examine other aspects of the surface confinement chemistry. In this paper, we report on the synthesis of multilayers of STA molecules on Ag(100) electrode surfaces formed by electrochemical polarization. Detailed spectroscopic and structural probes are utilized to confirm and explain the structures formed.

II. Experimental Section

Solutions were prepared in purified water (Milli-Q UV plus, 18.2 MΩ cm). The supporting electrolyte was 0.1 M $HClO_4$ (J. T. Baker, ULTREX II Ultrapure Reagent). α-Dodecatungstosilicate anion (STA), α-$SiW_{12}O_{40}^{4-}$, was prepared following published procedures[36] and recrystallized from purified water. The typical STA concentration was 0.5 mM. Ag substrates were formed from a Ag(100) single crystal (Monocrystals, Richmond Height, OH) etched according to published procedures using CrO_3/HCl solution.[37] Au(111) surfaces were prepared by annealing an Au-coated glass (Dirk Schröer Inc.) with a high-purity scientific grade H_2 flame prior to use.[38] After this treatment, Au(111) terraces with domain sizes larger than 100 nm were readily achieved. Freshly flame-annealed Pt wires were used as the counter electrode. A AuO wire was used as the reference electrode for STM measurements, a Ag/AgCl reference was used for the voltammetry, and a reversible hydrogen electrode in 0.1 M $HClO_4$ was used in X-ray reflectivity measurements. All potentials are reported relative to the Ag/AgCl reference (+0.20 vs SHE). Voltammetry was obtained using a Pine AFRDE-5 potentiostat and a two-compartment cell that was purged with Ar prior to use.

Quartz crystal microbalance (QCM) measurements were collected with a Maxtek model PM710 electrochemical thickness monitor (Maxtek Inc., Santa Fe Springs, CA). The working electrode potential was controlled by a AFRDE-5 potentiostat. The QCM cell was immersed in a water-jacketed beaker thermostated at room temperature, and solutions were purged with Ar prior to use. A continuous flow of Ar was kept above the solution surface when data were recorded. Au-coated AT cut quartz QCM crystals were purchased from Maxtek. A total thickness of 500−1000 Å of Ag was evaporated on top of the Au film in high vacuum at room temperature. These films were not annealed.

X-ray photoelectron spectroscopy (XPS) was performed on a Physical Electronics PHI 5400 XPS spectrometer equipped with a sample rotation stage. A polished Ag(100) single crystal was immersed into a solution containing 0.5 mM STA + 0.1 M $HClO_4$, and a potential of −0.1 V was applied. The potential was swept between +0.30 V and −0.60 V six times at a scan rate of 50 mV/s and poised at −0.10 V overnight (at least 16 h). After emersing the treated Ag sample at −0.6 V the sample was rinsed with Milli-Q water. The sample was then transferred through air to the spectrometer.

Scanning tunneling microscope (STM) images were obtained with a NanoScope III E electrochemical STM (ECSTM) equipped with a fluid cell (Digital Instruments, Santa Barbara, CA) or a Molecular Imaging STM. The tip was formed from a Pt/Ir wire coated with polyethylene except at the very end of the tip to minimize the Faradaic background current. Atomic resolution in situ STM images on untreated Ag(100) crystals revealed the expected (100) texture with at least 50 nm wide terraces.

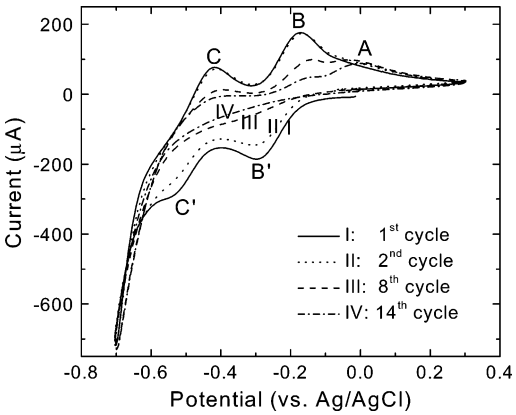

Figure 1. Cyclic voltammograms of 5 mM STA + 0.1 M $HClO_4$ electrolyte solution at a Ag(100) electrode for various numbers of scanning cycles. Curves I (solid line), II (dotted line), III (dashed line), and IV (dotted−dashed) correspond to the first, the second, the eighth, and the 14th cycles, respectively. Scan rate = 50 mV/s.

X-ray specular reflectivity measurements were carried out at the National Synchrotron Light Source (NSLS) at beam line ×22A using monochromatic X-rays with $\lambda = 1.20$ Å. The Ag(100) single crystal was oriented within 0.2° of the (100) crystallographic plane. After chemical polishing using CrO_3/HCl solution,[37] the sample was cleaned in H_2SO_4 and H_2O and transferred into an electrochemical X-ray scattering cell with a drop of water covering the surface. A body-centered tetragonal coordinate system was used to describe the reciprocal space vector, $Q = |H\vec{a}^* + K\vec{b}^* + L\vec{c}^*|$, where $a^* = b^* = 2\pi/a$, $c^* = 2\pi/\sqrt{2}a$. For Ag(100), $a = 2.889$ Å, and L is along the surface normal direction. All of the integrated intensities were measured with a 2 mm × 2 mm slit located 600 mm from the sample. The resulting resolution in the surface plane is larger than the intrinsic peak width for all measured reflections.

III. Results

3.1. CV on Ag(100). Figure 1 shows the time-dependent cyclic voltammograms from a Ag(100) electrode in 5 mM STA + 0.1 M $HClO_4$ electrolyte solution. Curve I shows the first cycle obtained immediately following exposure of the surface to the solution beginning from 0.0 V and extending to the negative potential region. This voltammogram shows two redox waves, labeled B/B′ and C/C′, with midpoint potential $E_{mid} = -0.23$ and −0.48 V, respectively. Here $E_{mid} = (E_a + E_c)/2$ and E_a and E_c are the anodic and cathodic peak potentials, respectively. The peak locations are in good accordance with those reported in our previous electrochemical studies of STA on Ag(111) electrode surfaces.[33]

Upon further potential cycling between +0.30 and −0.70 V, both the cathodic and anodic peak currents decrease gradually as shown in curves II, III, and VI in Figure 1. After the fourteenth cycle, as shown in curve VI, the cathodic waves (B′ and C′) disappear and only residual anodic current associated with peaks B and C remains. The Ag surface becomes more passivated after further potential cycling, and electron-transfer reaction across the interface becomes less facile, consistent with our previous work on Ag(111).[33] One anodic peak, positioned around 0 V (labeled A), grows at the expense of the two solution STA redox peaks. These phenomena were also observed for Ag(111) electrode surfaces, and the growth of peak A was

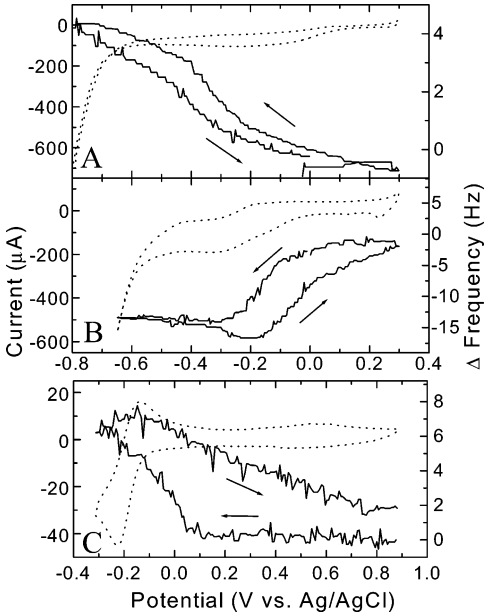

Figure 2. Current (dotted line) and frequency (solid) response of (A) a Ag QCM oscillator electrode in 0.1 M $HClO_4$, (B) a Ag QCM oscillator electrode in 0.25 mM STA + 0.1 M $HClO_4$, and (C) a Au QCM oscillator electrode in 0.1 mM STA + 0.1 M HF solution. Scan rate = 50 mV/s (A and B) and 25 mV/s (C).

attributed to the oxidation of decomposition of the reduced, adsorbed Ag−STA complex formed at a potential region more negative than −0.65 V.[33]

3.2. QCM Measurements. Figure 2 shows the current and frequency response of a Ag QCM electrode as a function of potential. In pure electrolyte solution, shown in Figure 2A, the oscillator frequency is invariant between +0.3 and 0.0 V, while the frequency starts to increase as the potential is swept negatively from 0.0 V. A small amount of cathodic current is recorded at around −0.1 V, which is likely due to reduction of residual oxygen dissolved in the solution. As the potential scan direction is reversed, a slight hysteresis is observed, and the frequency returns to its original value. The total frequency change in this region is +5 Hz. Since the AT cut quartz crystals we used have a mass coefficient of −17.7 ng/(cm^2·Hz), the total effective mass change at the Ag interface is −88.5 ng/cm^2. Assuming that this mass change can be attributed to the desorption of the anion, ClO_4^-, in the negative region, we can calculate the change in surface coverage using

$$\theta_{\text{anion}} = \frac{N_{\text{anion}}}{N_{\text{surface atom}}} = \frac{\Delta W_{\text{anion}}/\text{MW}_{\text{anion}}}{N_{\text{surface atom}}} \qquad (1)$$

where ΔW_{anion} is the effective mass change and N_i is the density of the *i*th species on the surface. Using this formula, we obtain $\theta_{ClO_4^-} = 0.39$. Interestingly, on Au(poly) in 0.1 M $HClO_4$ between 0.05 and 1 V vs RHE a mass change attributable to ClO_4^- adsorption of +73.0 ng/cm^2 was obtained.[39] With the experimental roughness factor of 1.4 used by these authors, $\theta_{ClO_4^-} = 0.25$ can be calculated.[39] The greater coverage of perchlorate on the Ag surface may reflect the greater affinity of the Ag surface for oxoanions.

In the presence of STA, a different trend in frequency change was observed as shown in Figure 2B. The potential scan starting at 0.0 V was swept to the negative region, and the frequency begins to *decrease* at the onset of cathodic current at −0.10 V, which corresponds to the reduction of STA in the solution. The change in frequency reaches a plateau at −0.30 V, where the cathodic current is also at its maximum value. During the reverse potential scan, the frequency drops about 2 Hz and then at −0.20 V begins to climb to the original value obtained prior to the potential sweep. Hysteresis between the forward and return potential scan is observed. The total observed frequency change is −15 Hz, which corresponds to an effective mass change of +266 ng/cm^2.

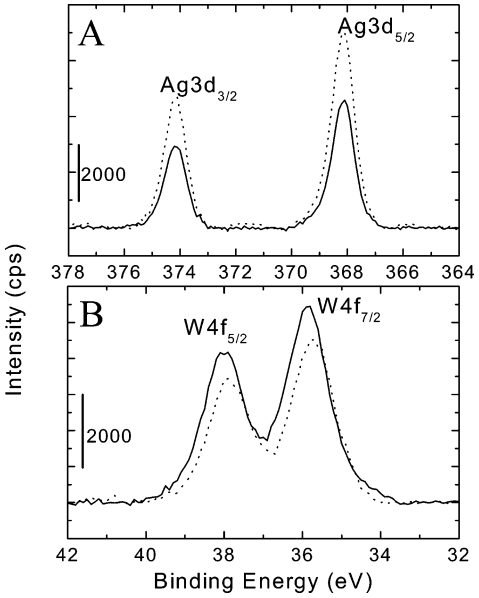

Figure 3. Multiplex XPS measurements in Ag 3d (A) and W 4f (B) areas of multilayers of α-$H_4SiW_{12}O_{40}$ on the Ag(100) sample. Solid and dotted lines correspond to electrochemically modified and dip-coated Ag surfaces, respectively.

In multiple measurements, the absolute frequency change observed for STA-containing solutions on the Ag QCM electrode ranged from −5 to −15 Hz. This inconsistency probably relates to differences in the Ag substrates evaporated on top of the Au-coated QCM crystals without annealing. Despite this inconsistency in the total frequency change, the frequency always decreased when the potential was swept negatively through the STA reduction region, which indicates that STA adsorbs onto the electrode with the negative potential excursion.

Figure 2C shows the frequency change observed on a Au QCM electrode in the presence of 0.1 mM STA + 0.1 M HF. In contrast to the situation with Ag, the frequency change is positive on cycling to negative potentials. A total frequency change of +7.8 Hz was measured on a Au electrode when the potential was scanned in the region from the positive end of the double layer region through the first one-electron reduction peak of STA. The positive change in frequency indicates net weight loss (ca. −140 ng/cm^2) on the Au electrode surface, which means STA molecules desorb from the electrode surface after one-electron reduction. The weight loss is equivalent to a coverage of $\theta_{\text{STA}} = 0.016$ under the assumption of a roughness factor equal to 1 for this Au surface. Kuhn and Anson observed that upon reduction $P_2W_{18}O_{62}^{6-}$ anions are similarly desorbed from Au.[4]

3.3. XPS. An XPS survey scan of the STA-modified Ag(100) electrode showed contributions from Ag, W, Si, O, and C. The presence of W and Si on the Ag surface indicates that STA molecules still stay on the Ag surface after the electrode is emersed from the solution and rinsed with water. To obtain the W to Ag peak ratios of the electrochemically treated STA on the Ag(100) sample, multiplex scan spectra were also collected, as shown in Figure 3 (solid line). For comparison purposes,

XPS analysis was also performed on a Ag(100) single crystal which was only immersed in 0.5 mM STA + 0.1 M $HClO_4$ solution overnight, emersed in air, and rinsed with 0.1 M $HClO_4$ solution (Figure 3, dotted line). For each modification, two different Ag(100) samples were analyzed, and the calculated areas under the W and Ag peaks in the two data sets were averaged.

The average ratio of the intensity of W 4f peaks divided by the spectrometer sensitivity factor for W (3.523)[40] to the intensity of the Ag 3d peaks divided by the Ag sensitivity factor (5.987)[40] of the electrochemically treated STA on the Ag(100) sample is 0.59. On the other hand, the intensity ratio of W to Ag for the STA/Ag(100) substrate without electrochemical treatment is 0.39, which is smaller than the one obtained from the STA/Ag(100) sample treated electrochemically. Therefore, qualitatively, the amount of STA deposited on the Ag surfaces after electrochemical cycling and potential poising is larger than the amount of STA on the Ag surfaces without potential treatment.

Figure 3 also shows that the position of the W peaks shifts by ca. −0.15 eV in the electrochemically treated STA/Ag(100) sample relative to the dipped sample. However, there is no shift evident in the position of the Ag or C peaks, which indicates that this shift is not due to charging during the XPS measurements. One possible origin of the shift is packing stabilization of the STA molecule.

3.4. STM. As reported in our previous studies,[29,32] a partial monolayer of STA is always observed immediately after the Ag electrode surface was immersed in 0.5 mM STA + 0.1 M $HClO_4$ solution under open circuit potential conditions (ca. +0.3 V). More ordered monolayers of STA can be formed by applying a potential more negative than the open circuit potential (ca. +0.05 V).[32]

Figure 4 shows a series of time-dependent STM images of a Ag (100) surface in 0.5 mM STA + 0.1 M $HClO_4$ solution at −0.1 V. Figure 4A was obtained right after the potential was held at −0.1 V. The dark and gray areas in this figure represent the bare Ag surface and the STA monolayer, respectively, while the bright domains (denoted with arrows) correspond to the newly formed islands on top of STA monolayers. These islands become larger with time after holding the potential at −0.1 V, as shown in Figure 4B−F. In Figure 4F, additional spots atop the second layer are observed.

Molecular resolution of the bright spots on these islands revealed features separated by ca. 11−12 Å. On the basis of the intermolecular spacing and the fact that no island growth is observed when a negative potential is applied on Ag surfaces in the solution without STA, these islands are associated with STA or STA-related products. The apparent height of the islands in these STM images is measured to be between 2.6 and 4.0 Å, which is smaller than the actual height of a STA molecule (ca. 10 Å). By way of comparison, a monolayer height of 5 Å was reported for a STA monolayer on a Ag(111) surface.[29] This discrepancy could be due to the tunneling effect of the STM tip arising from the particular choice of imaging parameters which is known to affect the apparent heights.[41]

To probe conditions required for multilayer formation, we performed measurements on Au surfaces in the absence and presence of a controlled amount of Ag^+.

Figure 5A shows a STM image obtained on a Au(111) electrode surface at +0.08 V in 0.5 mM STA solution in the absence of Ag^+. High-resolution images (not shown) of this surface revealed ordered domains of STA, which could also be observed without any potential control as soon as the surface was exposed to STA-containing solution.[31] When a potential more negative than the open circuit potential (ca. +0.45 V) was applied, ordered STA domains could be observed until ca. +0.05 V, which is the onset potential for the first one-electron reduction. At this potential, step edges evinced the "frizzy" features which are indicators of increased mobility of adsorbed STA molecules.[42] These frizzies became more pronounced at increasingly negative potentials as the STA molecules begin to desorb.

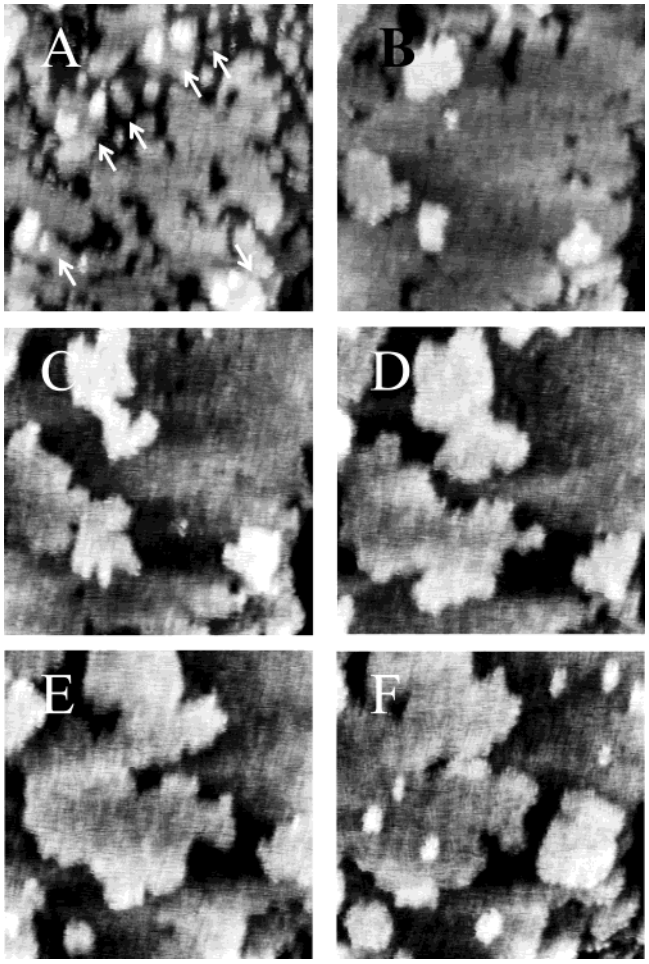

Figure 4. Series of 80 nm × 80 nm STM images of a Ag(100) surface in 0.5 mM STA + 0.1 M $HClO_4$ solution at −0.10 V: (A) $t = 0$ min; (B) $t = 9$ min; (C) $t = 15$ min; (D) $t = 24$ min; (E) = 30 min; (F) $t = 56$ min. $I_{set} = 0.97$ nA, and $E_{bias} = 192$ mV.

Figure 5B shows the surface observed at a potential of −0.16 V. A relatively large cathodic current is flowing at this potential, due to a combination of reduction of solution STA and oxygen reduction, since the solution in the STM cell was not degassed. The figure shows the presence of small isolated dotlike features. Unlike the behavior observed on Ag surfaces, these isolated small islands did not coalesce or increase in size when the negative potential was applied for a longer time. Because such features were not observed in the solution absent of STA with the same potential treatment, these isolated islands are also considered to be related to STA. Unfortunately, images could not be obtained beyond ca. −0.30 V due to the large cathodic current from both STA and H_2 reduction reactions. Upon sweeping the potential back to more positive values, the islands described above did not disappear. Domains of STA were observed surrounding those small isolated islands even when the potential was scanned up to +0.85 V.

To investigate the influence of Ag^+ on the formation of α-$SiW_{12}O_{40}^{4-}$ layers, STM measurements were conducted with

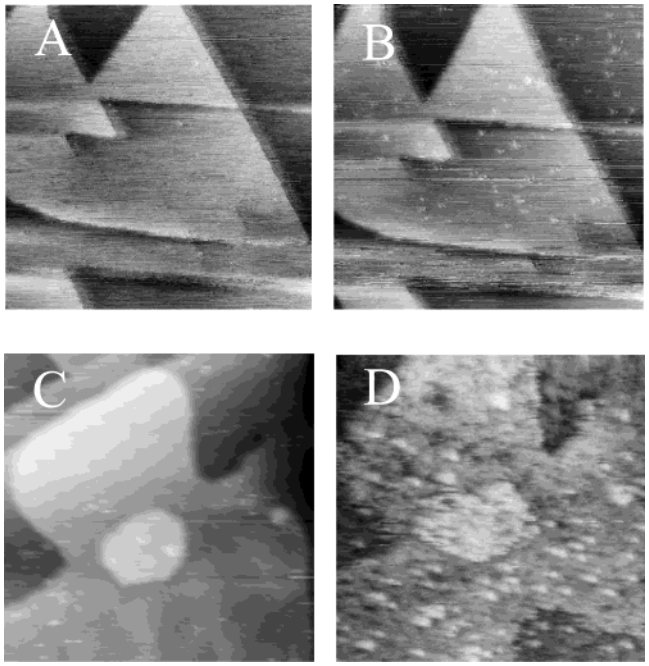

Figure 5. Series of 150 nm × 150 nm STM images of a Au(111) surface in 0.5 mM STA + 0.1 M H_2SO_4 solution (A and B) in the absence of Ag_2SO_4 and (C and D) in the presence of 0.01 mM Ag_2SO_4 at different potentials: (A) +0.08, (B) −0.16, (C) −0.03, and (D) −0.22 V.

the addition of a small amount of Ag^+ ions in 0.5 mM α-$H_4SiW_{12}O_{40}$ + 0.1 M H_2SO_4 solution on Au(111) surfaces. The amount of Ag^+ ions was controlled carefully because of the low solubility of the corresponding $Ag-SiW_{12}O_{40}$ salts. When only 0.01 mM Ag_2SO_4 was present in the solution, no precipitate was observed.

Initially following immersion of the Au surface into the α-$H_4SiW_{12}O_{40}$ solution containing 0.01 mM Ag_2SO_4, a $(\sqrt{3} \times \sqrt{7})$ structure was observed in the STM image at open circuit potential. This structure is undoubtedly the well-studied sulfate−water adlayer on the Au electrode surface.[43] When a more negative potential was applied, different structures, which involved STA and Ag^+, were observed depending on the applied potential. Due to the complexity of Ag underpotential deposition (UPD) structures in the potential range between 0.1 and 0.0 V,[44] we did not analyze atomic and molecular arrangements in this region.

Figure 5C is an STM image obtained from a Au surface immersed in a 0.5 mM α-$H_4SiW_{12}O_{40}$ + 0.1 M H_2SO_4 + 0.01 mM Ag_2SO_4 solution at a potential of −0.03 V. The image shows a series of clusters or small islands. The number and size of these islands grew as the potential reached −0.15 V, and achieved saturation at a potential of −0.22 V following a period of 30 min. Figure 5D is an STM image that shows the surface after this saturation was reached; this image was stable for at least 1 h. High-resolution images obtained at this potential revealed two types of domains. The first, small isolated islands, were similar to those observed without addition of Ag_2SO_4. The second type of domain was aggregates of spots with STA-like spacings of between 10 and 12 Å. On the basis of the spacing between these spots, we suggested that these features consist of STA or reduced STA species (α-$SiW_{12}O_{40}^{5-}$).

When potential was returned to more positive values, the two types of deposits on the surface behaved differently. While the aggregated STA-like species desorbed from the surface, the small isolated islands formed in the negative potential region

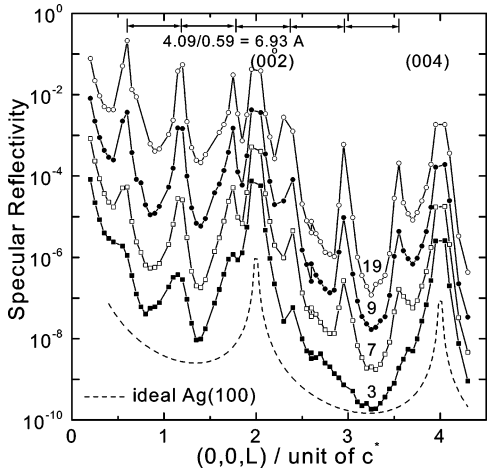

Figure 6. X-ray specular reflectivity profiles (solid lines) measured for STA multilayer growth on Ag(100) in 1.0 mM STA+ 0.1 M $HClO_4$ solution at −0.10 V after three potential cycles between +0.10 V and −0.50 V. The number of hours when the reflectivity profile was measured are 3 (filled square), 7 (empty square), 9 (filled circle), and 19 (empty circle), as given in the figure. The ideal Ag(100) data are represented in a dotted line, and the curves are offset for clarity.

did not. These features remained on the Au surface through continued application of a positive potential. This means that these island features are not simply the products of Ag deposition.

The small isolated islands are observed on the Au(111) electrode in the presence of STA with or without Ag^+ in solution. The formation of these small islands is not reversible when the potential is scanned back to the positive region. The identity of these features is still not understood. It is tentatively suggested that these small islands are the products of the reduction of STA in the presence of oxygen, which show greater affinity to the Au surface for reasons not readily apparent.

3.5. X-ray Reflectivity. The surface-normal structure at the solution/electrode interface can be determined by collecting the X-ray reflectivity profiles along the surface normal direction.[19] Figure 6 shows the evolution of the intensities of specular reflectivity measured along the Ag(100) surface-normal direction, *L*, as a function of time following poising the potential at −0.10 V in 1.0 mM STA + 0.1 M $HClO_4$ solution after three potential cycles between +0.10 V and −0.50 V.

The dashed line in Figure 6 shows the specular reflectivity profile for an ideally terminated Ag(100) surface, where the Bragg peaks are at even integers along the (0,0,*L*) direction. Between these Bragg peaks, the measured X-ray intensities are sensitive to the adsorbates on the surface. Extra peaks with a spacing of 0.59 (c^* is defined by the Ag(100) lattice constant of 4.09 Å) emerge and increase with time after holding the potential at −0.1 V (solid lines in Figure 6). The corresponding layer spacing in real space can be calculated from 4.09/0.59 = 6.93 Å, which is smaller than the molecular length along the S_4 axis (7.4 Å), suggesting a staggered packing sequence. The width of the peaks is inversely related to the number of $Ag^+-SiW_{12}O_{40}^{n-}$ layers. The increase of overall intensity in addition to the sharpening of the peaks shows the growth is in both lateral and vertical directions over a long period of time. Thus, the formation of the multilayer film is not layer-by-layer, but rather a 3D nucleation and growth process.

IV. Discussion

The results reported above provide strong evidence for a multilayer structure formed by STA on Ag electrodes at negative

potentials. In what follows, we address the conditions necessary for multilayer formation, the structure of the multilayer, and the reason for the negative potential requirement. We note generally, that the multilayer is likely formed from STA itself, since recent Raman measurements provide strong evidence that STA is present on the Ag surface throughout the addressable potential region.[35]

4.1. Conditions for Multilayer Formation. In previous reports, STM images showing monolayer structures of STA on Ag surfaces were obtained at a potential equivalent to or slightly more negative than the open-circuit potential. Aggregates or multilayer structures were never observed.[29−32] This potential range—+0.3 to +0.05 V for a Ag(100) surface—corresponds to the double-layer region for STA on Ag. Tang et al. also reported a STM image showing well-ordered monolayer structures of $AsMo_{11}VO_{40}^{4-}$ on the Au electrode at +0.7, which potential is more positive than the onset of the first two-electron reduction of solution $AsMo_{11}VO_{40}^{4-}$. [45] In general, as long as the potential is not scanned more negative than the onset of the first one-electron reduction of solution STA, monolayers of STA are preserved and no aggregation or multilayer is formed on top of the underlying STA monolayer.

However, at a potential more negative than the onset of the first one-electron reduction of solution STA (ca. −0.05 V), the STM, QCM, and X-ray reflectivity agree that additional material is deposited onto the STA-monolayer covered surface. This additional material is likely STA, because the ca. 1 nm spacings observed on the multilayer in STM images is that expected for this molecule. These STA islands are only stable in the negative potential region. From a series of higher resolution STM images consisting of multilayers of STA, it was observed that linearly changing the potential in a positive direction results in gradual dissolution of the islands. This dissolution was also inferred from the QCM measurements.

Interestingly, multilayer behavior was not observed on Au surfaces. Instead, both QCM and STM results indicate that STA is *desorbed* from the Au surface at negative potentials. Keita and co-workers also concluded from their QCM results that STA desorbs from Au surfaces at the potential where the one-electron reduction of STA occurres.[46]

4.2. Structure of the Multilayer. The oscillation patterns in Figure 6 are due to diffraction from the layered structure formed through the coagency of Ag and STA and will appear in the data only if there is a periodic component in the surface normal direction. The positions of the oscillation maxima obtained at −0.10 V after cycling the potential are different from what was observed on Ag(100) when the potential was held at +0.10 V without cycling the potential reported in our previous study.[32] In this latter case, only monolayers of STA were observed to form in both STM and X-ray reflectivity measurements.

Since the interlayer spacing calculated from X-ray reflectivity data (6.93 Å) is slightly smaller than the distance (7.4 Å) between the bottom and top layers of oxygen in a STA molecule with the C_4 axis normal to the Ag(100) surface, the STA molecules are likely in the hollow sites of the underlying layer. To have such a compact structure, charge neutralization seems to be necessary, which can be achieved by coadsorption of cations such as H^+ and Ag^+. Due to the large number of atoms that are possibly involved in the diffraction pattern, no specific model is given to describe the construction of the ordered layers.

In the STM measurements, the height difference between different layers of STA was found to be between 2.6 and 4 Å, which is again considerably smaller than that found from X-ray reflectivity measurements. The origin of this discrepancy is likely due to differences in tunneling rates between different layers of STA on the surface. The higher layers will likely be more insulating, resulting in a closer approach of the tip to the surface relative to lower layers or the bare surface.

4.3. Origin of Multilayer Formation in the Negative Potential Region. The results presented above provide strong evidence that excursion of potential into the region around the first observable redox peak in the STA/Ag system leads to the formation of STA-containing multilayers on the Ag surface. This multilayer formation process appears to have much in common with that found in other anion−cation multilayer systems formed using STA or related polyoxometalates. However, the results presented here are the first that definitively show that this multilayer exhibits order normal to the electrode surface. Both Ag^+ and STA seem to be necessary components in order to observe multilayer formation, as a similar process does not occur on Au or other surfaces. This suggests that Ag^+ is the cation in the multilayer. The formation of cationic adlayers of Ag^+ atop polyoxometalate adlayers has been previously discussed.[9]

There are two possible explanations for the role of negative potentials in stabilizing these multilayers. First, the islands on top of the monolayer of STA could be composed of the one-electron reduced products of STA. These reduced STA species (α-$SiW_{12}O_{40}^{5-}$) are not stable once they are reoxidized at positive potential. Second, the negative potential could stabilize a cationic component of the solution—likely Ag^+—which then helps to maintain the anionic STA species on the surface.

We note that the growth of STA multilayers occurs only on Ag electrodes or on Au electrodes in the presence of Ag^+ in the negative potential region. This suggests strongly the multilayer is not simply composed of one-electron reduced STA species, since these occur on Au without Ag^+ addition. On Ag surfaces at equilibrium, a small amount of Ag^+ is present near the Ag surface in acid media due to the finite solubility of Ag. Ag^+ ions exist initially at a concentration of ca. 10^{-7} M in the acidic conditions under which these measurements were performed. Thus, Ag^+ is available near the Ag surface, even without explicit addition of the species to the solution. We conclude that negative potential can stabilize Ag^+, which facilitates holding STA or reduced STA species together on top of STA monolayers via electrostatic means.

Why should Ag^+ be stable at negative potentials near the Ag surface? We note that the silver salts of Keggin type molecules are highly insoluble in aqueous media.[47] Negative potentials help to attract and stabilize Ag^+ ions and thus more $Ag-SiW_{12}O_{40}$ complexes can be built-up upon negative potential excursion. Reduction of Ag^+ which would occur on unpassivated surfaces may be inhibited by the presence of the complex already on the surface.

There is support for the idea that cathodic treatment can stabilize the heteropolyanions on other electrode surfaces. For example, Ilangovan et al. prepared monomeric molybdate(VI)-modified glassy carbon electrode following pretreatment of the glassy carbon surface by precathodization methods.[48,49] Following exposure of the electrode to the Mo(VI) species, these authors reported the existence of mixed-valent Mo(VI)/Mo(V) complexes on the surface as indicated by XPS. The authors proposed that the formation of Mo(V) during Mo(VI) adsorption occurs through simultaneously oxidation of alcohol functional groups on the glassy carbon electrode created during the precathodization treatment.

In conclusion, we have shown that STA forms multilayers on the Ag surface and on other surfaces in the presence of Ag. The STA apparently stabilizes the Ag^+ cation, which electro-

statically assembles with the STA anion, or the one-electron reduced species to form ordered multilayers. In contrast to other electrostatically assembled multilayer systems, those formed here exhibit considerable order, the exploitation of which will be a focus of future work.

Acknowledgment. J.K. acknowledges a graduate fellowship from the Chemistry Department at the University of Illinois. J.X.W. acknowledges the support by U.S. Department of Energy, Divisions of Chemical and Material Sciences, under Contract No. DE-AC02-98CH10886. This work was funded by the National Science Foundation (Grant CHE 02-37683), which is gratefully acknowledged.

References and Notes

(1) Mizuno, N.; Misono, M. *Chem. Rev.* **1998**, *98*, 199−217.
(2) Sadakane, M.; Steckhan, E. *Chem. Rev.* **1998**, *98*, 219−237.
(3) Katsoulis, D. E. *Chem. Rev.* **1998**, *98*, 359−387.
(4) Kuhn, A.; Anson, F. C. *Langmuir* **1996**, *12*, 5481−5488.
(5) Ichinose, I.; Tagawa, H.; Mizuki, S.; Lvov, Y.; Kunitake, T. *Langmuir* **1998**, *14*, 187−192.
(6) Yitzchaik, S.; Marks, T. J. *Acc. Chem. Res.* **1996**, *29*, 197−202.
(7) Ingersoll, D.; Kulesza, P. J.; Faulkner, L. R. *J. Electrochem. Soc.* **1994**, *141*, 140−147.
(8) Cheng, L.; Niu, L.; Gong, J.; Dong, S. J. *Chem. Mater.* **1999**, *11*, 1465−1475.
(9) Kuhn, A.; Mano, N.; Vidal, C. *J. Electroanal. Chem.* **1999**, *462*, 187−194.
(10) Cheng, L.; Cox, J. A. *Chem. Mater.* **2002**, *14*, 6.
(11) Sun, C. Q.; Zhang, J. D. *Electrochim. Acta* **1998**, *43*, 943−950.
(12) Cheng, L.; Liu, J. Y.; Dong, S. J. *Anal. Chim. Acta* **2000**, *417*, 133−142.
(13) Wang, B.; Dong, S. *J. Electroanal. Chem.* **1992**, *328*, 245−257.
(14) Tang, Z. Y.; Liu, S. Q.; Wang, E. K.; Dong, S. J.; Wang, E. B. *Langmuir* **2000**, *16*, 5806−5813.
(15) Zhang, B. L.; Wang, E. K. *J. Electroanal. Chem.* **1995**, *388*, 207−213.
(16) Cheng, Z. L.; Cheng, L.; Dong, S. J.; Yang, X. R. *J. Electrochem. Soc.* **2001**, *148*, E227−E232.
(17) Cheng, L.; Dong, S. *J. Electroanal. Chem.* **2000**, *481*, 168−176.
(18) Liu, S. Q.; Tang, Z.; Wang, Z. X.; Peng, Z. Q.; Wang, E. K.; Dong, S. J. *J. Mater. Chem.* **2000**, *10*, 2727−2733.
(19) Decher, G. *Science* **1997**, *277*, 1232−1237.
(20) Huc, V.; Bourgoin, J. P.; Bureau, C.; Valin, F.; Zalczer, G.; Palacin, S. *J. Phys. Chem. B* **1999**, *103*, 10489−10495.
(21) Yang, H. C.; Aoki, K.; Hong, H. G.; Sackett, D. D.; Arendt, M. F.; Yau, S. L.; Bell, C. M.; Mallouk, T. E. *J. Am. Chem. Soc.* **1993**, *115*, 11855−11862.
(22) Hatzor, A.; Moav, T.; Cohen, H.; Matlis, S.; Libman, J.; Vaskevich, A.; Shanzer, A.; Rubinstein, I. *J. Am. Chem. Soc.* **1998**, *120*, 13469−13477.
(23) Ulman, A. *Chem. Rev.* **1996**, *96*, 1533−1554.
(24) Katz, H. E. *Chem. Mater.* **1994**, *6*, 2227−2232.
(25) Tour, J. M.; Jones, L.; Pearson, D. L.; Lamba, J. J. S.; Burgin, T. P.; Whitesides, G. M.; Allara, D. L.; Parikh, A. N.; Atre, S. V. *J. Am. Chem. Soc.* **1995**, *117*, 9529−9534.
(26) Kohli, P.; Taylor, K. K.; Harris, J. J.; Blanchard, G. J. *J. Am. Chem. Soc.* **1998**, *120*, 11962−11968.
(27) Joo, S. W.; Han, S. W.; Kim, K. *Langmuir* **2000**, *16*, 5391−5396.
(28) Lin, W. B.; Lin, W. P.; Wong, G. K.; Marks, T. J. *J. Am. Chem. Soc.* **1996**, *118*, 8034−8042.
(29) Ge, M.; Zhong, B.; Klemperer, W. G.; Gewirth, A. A. *J. Am. Chem. Soc.* **1996**, *118*, 5812−5813.
(30) Ge, M.; Gewirth, A. A.; Klemperer, W. G.; Wall, C. G. *Pure Appl. Chem.* **1997**, *69*, 2175−2179.
(31) Ge, M.; Niece, B. K.; Wall, C. G.; Klemperer, W. G.; Gewirth, A. A. *Mater. Res. Soc. Symp. Proc.* **1997**, *451*, 99−108.
(32) Lee, L.; Wang, J. X.; Adzic, R. R.; Robinson, I. K.; Gewirth, A. A. *J. Am. Chem. Soc.* **2001**, *123*, 8838−8843.
(33) Lee, L.; Gewirth, A. A. *J. Electroanal. Chem.* **2002**, *522*, 11−20.
(34) Kim, J.; Gewirth, A. A. *Langmuir* **2003**, *19*, 8934−8942.
(35) Teague, C. M.; Li, X.; Biggin, M. E.; Lee, L.; Kim, J.; Gewirth, A. A. *J. Phys. Chem. B* **2004**, *108*, 1974−1985.
(36) Teze, A.; Herve, G. *Inorg. Synth.* **1990**, *27*, 85−96.
(37) Smolinski, S.; Zelenay, P.; Sobkowski, J. *J. Electroanal. Chem.* **1998**, *442*, 41−47.
(38) Will, T.; Dietterle, M.; Kolb, D. M. In *Nanoscale Probes of the Solid/Liquid Interface*; Gewirth, A. A., Siegenthaler, H., Eds.; Kluwer Academic Publisher: Dordrecht, The Netherlands, 1995; pp 137−162.
(39) Uchida, H.; Ikeda, N.; Watanabe, M. *J. Electroanal. Chem.* **1997**, *424*, 5−12.
(40) Chastain, J., Ed. *Handbook of X-ray Photoelectron Spectroscopy*; Perkin-Elmer: Eden Prairie, MN, 1992.
(41) Siegenthaler, H. In *Scanning Tunneling Microscopy II*, 2nd ed.; Guntherodt, H.-J., Wiesendanger, R., Eds.; Springer: New York, 1995; p 7.
(42) Giessen, M.; Dietterle, M.; Stapel, D.; Ibach, H.; Kolb, D. M. *Surf. Sci.* **1997**, *384*, 168.
(43) Magnussen, O. M.; Hagebock, J.; Hotlos, J.; Behm, R. J. *Faraday Discuss.* **1992**, *94*, 399−400.
(44) Chen, C. H.; Vesecky, S. M.; Gewirth, A. A. *J. Am. Chem. Soc.* **1992**, *114*, 451−458.
(45) Tang, Z. Y.; Liu, S. Q.; Wang, E. K.; Dong, S. J. *Langmuir* **2000**, *16*, 4946−4952.
(46) Keita, B.; Nadjo, L.; Belanger, D.; Wilde, C. P.; Hilaire, M. *J. Electroanal. Chem.* **1995**, *384*, 155−169.
(47) Kinne, M.; Barteau, M. A. *Surf. Sci.* **2000**, *447*, 105−111.
(48) Ilangovan, G.; Pillai, K. C. *Langmuir* **1997**, *13*, 566−575.
(49) Ilangovan, G.; Pillai, K. C. *J. Electroanal. Chem.* **1997**, *431*, 11−14.